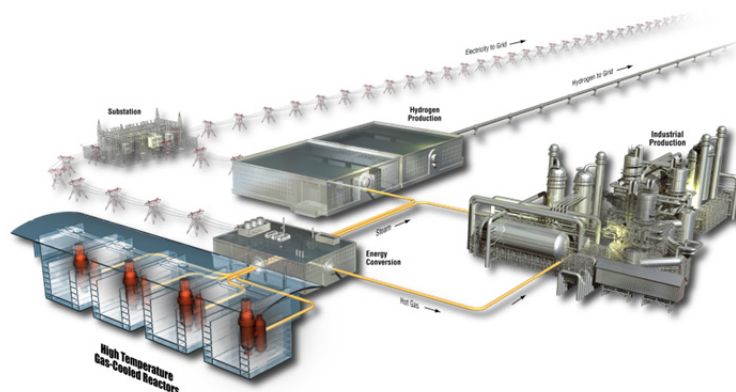


Super-Homogenization-Corrected Cross-Section Generation for High-Temperature Reactors

Sonat Sen
Andrew Hummel
Hikaru Hiruta

March 2017

The INL is a
U.S. Department of Energy
National Laboratory
operated by
Battelle Energy Alliance



DISCLAIMER

This information was prepared as an account of work sponsored by an agency of the U.S. Government. Neither the U.S. Government nor any agency thereof, nor any of their employees, makes any warranty, expressed or implied, or assumes any legal liability or responsibility for the accuracy, completeness, or usefulness, of any information, apparatus, product, or process disclosed, or represents that its use would not infringe privately owned rights. References herein to any specific commercial product, process, or service by trade name, trade mark, manufacturer, or otherwise, does not necessarily constitute or imply its endorsement, recommendation, or favoring by the U.S. Government or any agency thereof. The views and opinions of authors expressed herein do not necessarily state or reflect those of the U.S. Government or any agency thereof.

Super-Homogenization-Corrected Cross-Section Generation for High-Temperature Reactors

**Sonat Sen
Andrew Hummel
Hikaru Hiruta**

March 2017

**Idaho National Laboratory
INL ART TDO Program
Idaho Falls, Idaho 83415**

<http://www.inl.gov>

**Prepared for the
U.S. Department of Energy
Office of Nuclear Energy
Under DOE Idaho Operations Office
Contract DE-AC07-05ID14517**

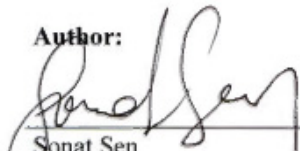
INL ART TDO Program

Super-Homogenization-Corrected Cross-Section Generation for High-Temperature Reactors

INL/EXT-17-41516
Revision 0

March 2017

Author:


Sonat Sen
INL ART TDO Staff Scientist /Engineer

3/30/2017
Date

Technical Reviewer: (Confirmation of mathematical accuracy, and correctness of data and appropriateness of assumptions.)


Hans D. Gougar
ART INL Director

3/30/2017
Date

Approved by:


Diane V. Croson
Deputy Director, INL ART TDO

3/30/17
Date


Michelle T. Sharp
INL ART TDO Quality Engineer

3/30/2017
Date

SUMMARY

Deterministic full reactor core simulators require homogenized group constants covering the operating and transient conditions over the entire lifetime of the core. Traditionally, the homogenized group constants are generated using lattice physics code over an assembly or, in the case of prismatic high-temperature reactors (HTRs), a block. In the case of strong absorbers that cause strong local depressions on the flux profile, special techniques, such as super-homogenization (SPH) are required during homogenization over a large volume. Fuel blocks with burnable poisons or control rod blocks are examples of such cases.

A hypothetical prismatic HTR core is modeled with the Serpent Monte Carlo code as the reference calculation to validate the experimental homogenized group constant generation methodology described in this report. The continuous-energy Monte Carlo method is capable of capturing all of the necessary nuclear physics in high fidelity and in three dimensions, thus allowing it to be used to assess the accuracy of the more approximate but generally faster running lattice physics codes such as DRAGON.

The DRAGONv5 deterministic code has been used to perform several two-dimensional lattice physics calculations for the hypothetical HTR prismatic core design. The different lattice models constitute so-called supercell (SC) arrangements of fuel blocks, control rod blocks, and graphite blocks. These SCs were chosen based on reactor symmetry, with the intent that the cross sections generated for a given central node (block) could be extended to all nodes in the problem that share common symmetry. Even though it does not fully cover the heterogeneity of the full core, a seven-block supercell with reflective boundary conditions has proven to produce adequate results for the full-core calculations. The results from all the models generated with DRAGONv5 are validated against the corresponding high fidelity Serpent model.

The results showed that the spatial convergence of a deterministic code is especially important when the local strong absorbers are present. Therefore, significant effort is required to spatially converge the SC models. The results of the full-core calculations using Idaho National Laboratory's nodal solver INSTANT are compared to the reference two-dimensional Serpent Monte Carlo solutions.

CONTENTS

| | |
|---|----|
| SUMMARY | v |
| ACRONYMS | ix |
| 1. INTRODUCTION | 1 |
| 2. MONTE CARLO CALCULATIONS | 1 |
| 2.1 Full-Core Calculations | 1 |
| 2.2 Two-dimensional Serpent Models | 4 |
| 3. HETEROGENEOUS LATTICE CALCULATIONS | 5 |
| 3.1 Geometric Models | 6 |
| 3.2 Spatial Convergence Study | 9 |
| 3.3 DRAGON Cross-Section Generation | 14 |
| 4. HTR FULL-CORE SIMULATION APPLYING SPH METHOD | 17 |
| 4.1 SPH Test Problem Performed with a Seven-Node HTR Supercell Model | 18 |
| 4.2 Preliminary Results for the Simplified Full-Core HTR Calculations with SPH Procedure | 22 |
| 5. CONCLUSIONS | 25 |
| 6. REFERENCES | 25 |

FIGURES

| | |
|--|----|
| Figure 1. SPHTR Serpent full-core model (XY view): CRs withdrawn | 2 |
| Figure 2. SPHTR Serpent full-core model (XY view): CRs inserted | 3 |
| Figure 3. 2D heterogeneous fuel block model with reflective boundary conditions | 4 |
| Figure 4. 2D full-core Serpent model of SPHTR | 5 |
| Figure 5. Full-core schematic of different SC arrangements | 7 |
| Figure 6. SC configurations, as shown in Figure 5, for generating homogeneous cross sections | 8 |
| Figure 7. Dragon infinite multiplication factor (k_{inf}) versus spatial discretization for a single fuel pin | 10 |
| Figure 8. Converged single fuel pin mesh | 10 |
| Figure 9. DRAGON k_{inf} versus spatial discretization for a fuel block without BP | 11 |
| Figure 10. Converged mesh for a single fuel block without BP | 11 |
| Figure 11. DRAGON k_{inf} versus spatial discretization for a fuel block with BP | 12 |
| Figure 12. Converged mesh for a single fuel block with BP | 12 |
| Figure 13. Serpent model of a single fuel block with BP and CR | 13 |

| | |
|---|----|
| Figure 14. DRAGON k_{inf} versus spatial discretization for a fuel block with BP and CR. | 13 |
| Figure 15. Converged mesh for a single fuel block with BP and CR. | 14 |
| Figure 16. The proposed SPH process for the HTR full-core calculations. | 18 |
| Figure 17. Seven-node modular HTR gas-cooled reactor SC model: (a) HELIOS-2 model and (b) INSTANT model. | 19 |
| Figure 18. Eigenvalue convergence behavior during the SPH factor iteration. | 20 |
| Figure 19. Reaction rates convergence behavior during the SPH factor iteration: (a) absorption rate and (b) fission rate. | 20 |
| Figure 20. Convergence behavior of SPH equivalence factors. | 21 |
| Figure 21. The process for the seven-node test problem with SPH corrections. | 21 |
| Figure 22. The simplified 2D HTR test geometry (SPHTR). | 22 |

TABLES

| | |
|---|----|
| Table 1. Characteristics of SPHTR. | 3 |
| Table 2. Serpent one-group neutron flux and reaction rates for different blocks normalized to one fission per second. | 5 |
| Table 3. Major geometry specifications for DRAGON SC lattice calculations. | 7 |
| Table 4. Material number densities used in DRAGON lattice calculations. | 8 |
| Table 5. DRAGON volume-integrated fluxes and homogeneous fission and absorption reaction rates of the central block for different SCs with absorber rods fully inserted. | 15 |
| Table 6. DRAGON volume-integrated fluxes and homogeneous fission and absorption reaction rates of the central block for different SCs with absorber rods fully withdrawn. | 16 |
| Table 7. Volume integrated fluxes and homogeneous fission and absorption reaction rates of the central block in 1 energy group for different SCs with absorber rods fully withdrawn | 16 |
| Table 8. Infinite multiplication factors for heterogeneous DRAGON SC calculations. | 17 |
| Table 9. Lower energy boundaries for the eight-group structure. | 19 |
| Table 10. Comparison of reaction rates calculated with and without SPH corrections. | 22 |
| Table 11. Comparison of INSTANT and DRAGON results for each rodged SC. | 23 |
| Table 12. Comparison of INSTANT and DRAGON results for each unrodged SC. | 23 |
| Table 13. Comparison of k_{eff} in the unrodged case. | 23 |
| Table 14. Comparison of k_{eff} in the rodged case. | 24 |
| Table 15. Comparison of INSTANT and Serpent reaction rates in 2D full-core models with control rods withdrawn. | 24 |

ACRONYMS

| | |
|-------|---|
| 2D | two-dimensional |
| 3D | three-dimensional |
| ART | Advanced Reactor Technologies |
| BP | burnable poison |
| BTE | Boltzmann transport equation |
| CR | control rod |
| He | helium |
| HTR | high-temperature reactor |
| HTTR | high-temperature test reactor |
| LWR | light water reactor |
| MHTGR | Modular High Temperature Gas-cooled Reactor |
| SC | supercell |
| SPH | super homogenization |
| SPHTR | Super-Homogenization High-Temperature Reactor |
| TRISO | tristructural-isotropic |

Super-Homogenization-Corrected Cross-Section Generation for High-Temperature Reactors

1. INTRODUCTION

Deterministic full reactor core simulators require homogenized group constants covering the operating and transient conditions over the entire lifetime of the core. Traditionally, the homogenized group constants are generated using lattice physics code over an assembly or, in the case of prismatic high temperature reactors (HTRs), a block. In the case of strong absorbers that cause strong local depressions on the flux profile, special techniques are required during homogenization over a large volume. Fuel blocks with burnable poisons (BPs) or control rod (CR) blocks are examples of such cases.

Over the past several decades, a tremendous number of studies have been performed to improve the accuracy of full-core calculations through the homogenization procedure. However, those studies were mostly performed for light-water reactor analyses; thus, the previous studies may not be directly applicable to advanced thermal reactors such as HTRs. The longer migration area of neutrons in graphite moderated cores, and the presence of strongly anisotropic absorbers within HTR fuel elements requires a different approach to lattice physics calculations, even when using a SuPer-Homogenization (SPH) correction method already proven for LWR analysis. This report presents the application of the super-homogenization correction method to a hypothetical HTR core.

2. MONTE CARLO CALCULATIONS

The continuous-energy Monte Carlo method is capable of capturing all of the nuclear reactions in high fidelity and in three dimensions, thus allowing it to be used to assess the fidelity of the simpler and generally faster running lattice physics codes such as DRAGON. The use of the Monte Carlo method for homogenized group constant generation for deterministic steady state or transient full core calculations became more common during the last decade. The practical applications, however, are still limited by the high computational cost. The homogenized group constant generation for steady state and transient full core calculations usually requires solving the local heterogeneous transport problem thousands of times to cover all fuel types and operating conditions over the lifetime of the core. On the other hand, using Monte Carlo lattice physics codes for generating the homogenized group constants also allows running transport simulations for the full-scale heterogeneous system, which provides the reference solutions for the validation of the calculation scheme.

The Serpent code [1], which has been developed at the VTT Technical Research Center of Finland since 2004, is used in the analysis. The spatial homogenization based on the Monte Carlo method was the original incentive for the development of the Serpent code, and the methodology for the homogenization can be found in [2]. The basic fundamentals of spatial homogenization can be found in [3,4] and in most textbooks on reactor theory (such as [5,6,7]).

A smaller and simpler High Temperature Gas-cooled Reactor (HTR) model, termed the SPHTR, was developed for this study to demonstrate the capabilities and efficacy of the spatial homogenization method presented in this report.

2.1 Full-Core Calculations

The Super-Homogenization High-Temperature Reactor (SPHTR) toy model developed for this report is a prismatic HTR with two fuel types differing only by enrichment, 14.5% and 15.5%, and loaded into the first and second rings, respectively, of a two-ring core. The Serpent model of SPHTR is illustrated in Figure 1 and Figure 2, with control rods withdrawn and inserted, respectively. The center block has three control rods. The first and second rings have 12 fuel blocks in each axial layer. Axially the active core has two layers. The fuel blocks contain 33 annular fuel compacts; the geometry and the dimensions of the fuel

compacts are same as in the Japanese high-temperature test reactor (HTTR) [8]. For simplicity, the center of the fuel blocks is modeled as graphite. The inner ring fuel blocks contain two BP channels on the periphery and one helium (He) channel, while the outer fuel blocks each contain one BP channel and two He channels. The tristructural-isotropic (TRISO) fuel exists as annular compacts with He gas in the center; a uniform packing fraction of 0.30 is used for all compacts. The six CR and shutdown rod blocks are located in the corners of the second ring. The CR design is considered to be the same as HTTR. Two rings of graphite reflector blocks surround the active core. A single layer of graphite reflector blocks is located at the top and bottom of the active core.

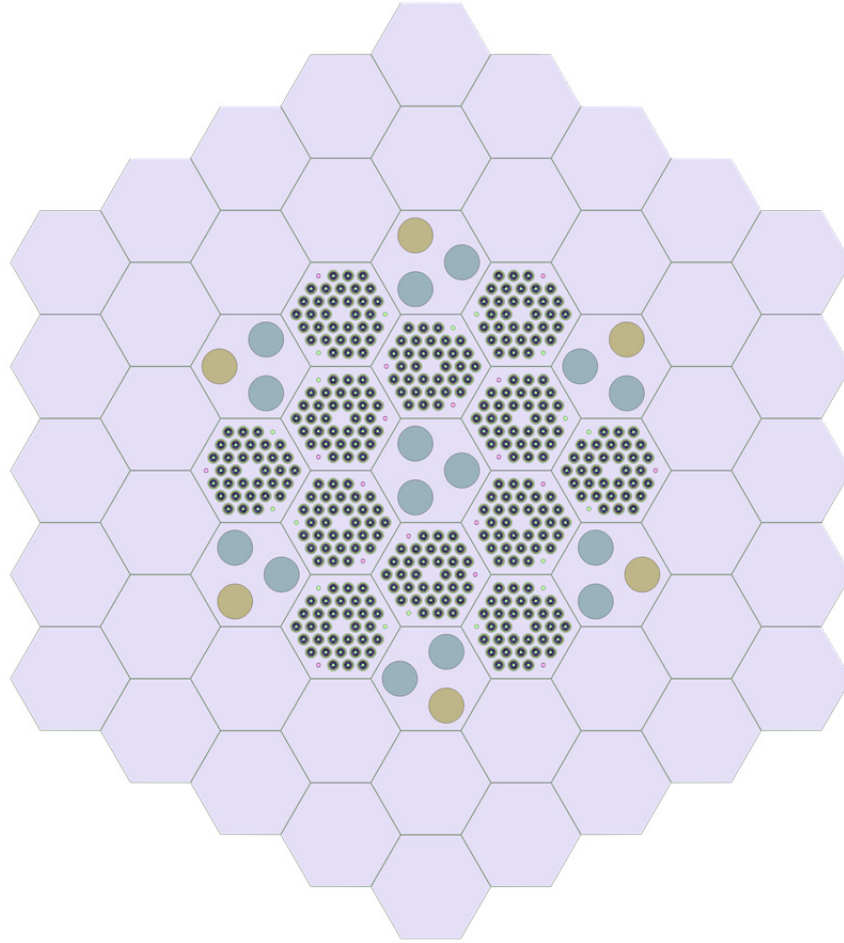


Figure 1. SPHTR Serpent full-core model (XY view): CRs withdrawn.

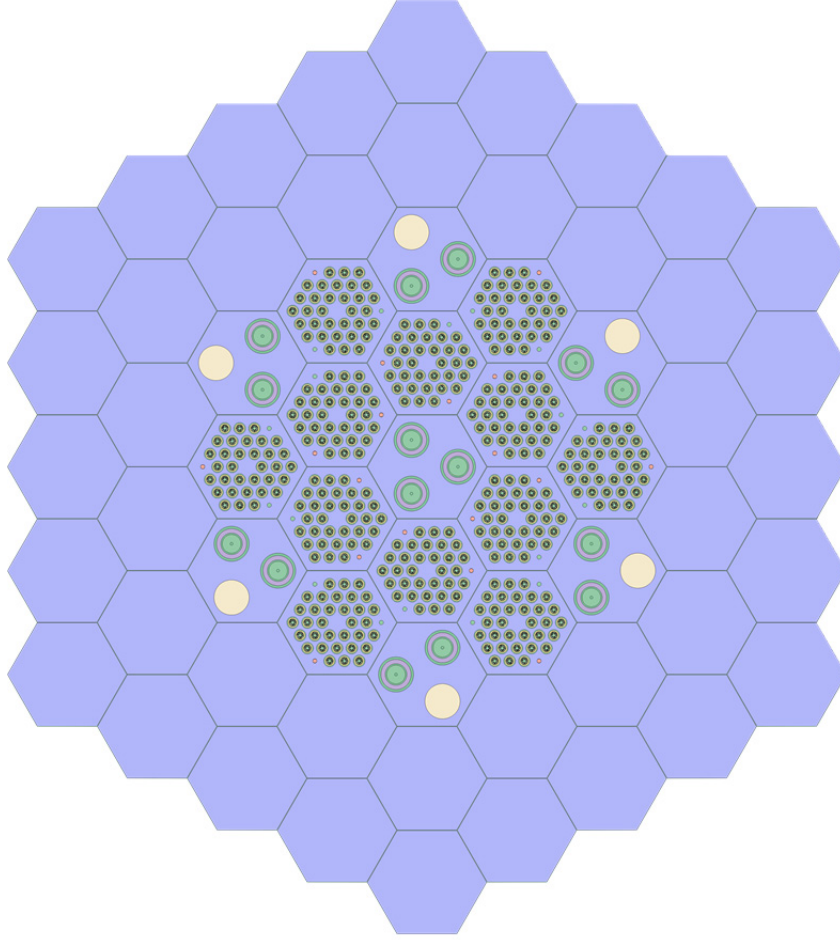


Figure 2. SPHTR Serpent full-core model (XY view): CRs inserted.

The calculations are performed at 900 K isothermal temperatures. The reactor is critical ($k_{eff} = 0.99995 \pm 0.00004$) when the CRs are inserted about 10 cm from the top of the upper fuel blocks. The CRs are withdrawn to the top of the top reflector ($k_{eff} = 1.05894 \pm 0.00004$) and inserted to the bottom of the bottom fuel block ($k_{eff} = 0.680243 \pm 0.00043$).

Table 1. Characteristics of SPHTR.

| Parameters | Value |
|---|-------------------------------|
| Power (MW) | 10.0 |
| Average fuel block power density (W/cm ³) | 7.3 |
| Number of fuel blocks | 24 |
| Block flat-to-flat (cm) | 36.0 |
| Gap between the blocks (cm) | 0.2 |
| Fuel compact radius (cm) | 2.05 |
| Fuel compact inner radius/outer radius (cm) | 0.5/1.3 |
| TRISO-coated fuel particle coatings radii (cm) | 0.03/0.036/0.039/0.0415/0.046 |
| BP pin radius (cm) | 0.7 |
| He channel radius (cm) | 0.75 |
| Control/shutdown rod radius (cm) | 6.15 |

The previous studies [9,10] showed that supercells (SCs) containing one ring of hex blocks surrounding the hex block in consideration with reflective boundary conditions could appropriately model the reactor configuration, even though they do not contain all the geometric features of the full core. Five SCs are identified in the SPHTR configuration:

1. The central CR block with its respective neighbors
2. The fuel blocks in the first ring and their respective neighbors
3. The fuel blocks in the second ring and their respective neighbors
4. The control and shutdown rod blocks with their respective neighbors
5. The graphite reflector block with its respective neighbors.

Note that this definition of SC for the graphite reflector is assumed to be representative for the outer graphite reflector blocks.

The 3D Monte Carlo full-core calculations are used as the reference solution for the validation of the calculation methodology. Two-dimensional (2D) full-core and infinite-medium heterogeneous single block (as shown in Figure 3) Monte Carlo calculations are also performed for the validation of the lattice physics models. Note that the fuel block shown in Figure 3 is slightly different than the fuel blocks shown in Figure 1 and Figure 2. The 2D infinite-medium Serpent model fuel block is adjusted from the original block only to match the DRAGONv5 models used in the lattice physics calculations, as described in the next section.

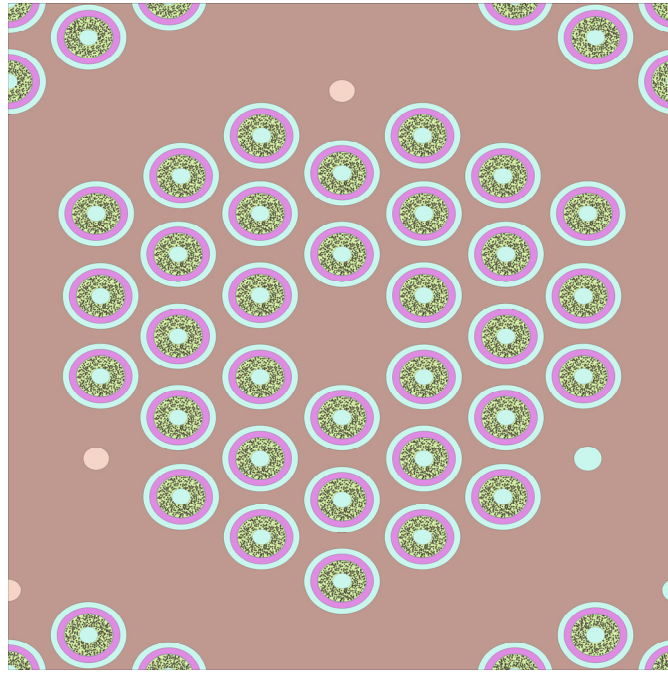


Figure 3. 2D heterogeneous fuel block model with reflective boundary conditions.

2.2 Two-dimensional Serpent Models

Two-dimensional full-core Serpent models are created for validation of the calculation methodology since the SPH corrected group constants are used in the two-dimensional INSTANT full-core model as described in section 4.2.

The Serpent model is actually three-dimensional (3.9 cm in height) for not making an approximation on the double heterogeneity of the TRISO particles in the fuel compact, however, reflective boundary

condition is applied in the 3rd dimension to mimic the 2D effects. Figure 4 illustrates the 2D full-core Serpent model of SPHTR with the control rods totally withdrawn. Another advantage of having 2D full-core models is to be able to generate the homogenized group constants directly from a Monte Carlo simulation, which would include the full heterogeneity of the core and the individual blocks at the same time.

Table 2 presents the one group neutron flux and the homogenized fission and absorption reaction rates calculated using 2D full-core Serpent model. The corresponding supercell for each block type is given in parenthesis. Note that these results are normalized to a fission rate equal to one.

Table 2. Serpent one-group neutron flux and reaction rates for different blocks normalized to one fission per second.

| Parameter | Central CR Block (SC1) | Inner Fuel Block (SC2) | Outer Fuel Block (SC3) | Outer CR Block (SC4) | Graphite Reflector Block (SC5) |
|------------------------------------|------------------------|------------------------|------------------------|----------------------|--------------------------------|
| Flux (n/cm-s) | 4.8450E+01 | 4.3361E+01 | 3.6467E+01 | 3.4210E+01 | 5.0660E+02 |
| Fission Rate (s ⁻¹) | 0.0000E+00 | 8.2905E-02 | 8.3814E-02 | 0.0000E+00 | 0.0000E+00 |
| nuFission Rate (s ⁻¹) | 0.0000E+00 | 2.0221E-01 | 2.0441E-01 | 0.0000E+00 | 0.0000E+00 |
| Absorption Rate (s ⁻¹) | 2.5272E-03 | 1.4151E-01 | 1.2967E-01 | 2.6821E-03 | 8.6583E-02 |

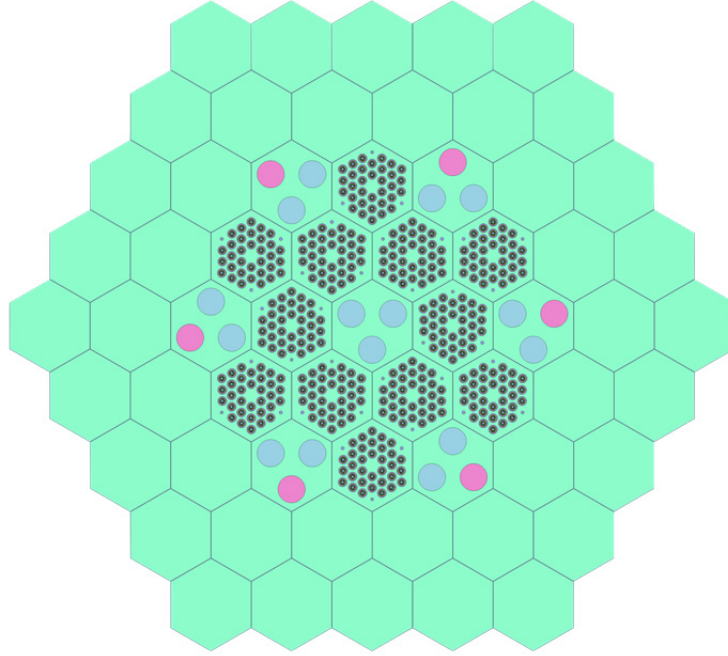


Figure 4. 2D full-core Serpent model of SPHTR.

3. HETEROGENEOUS LATTICE CALCULATIONS

The DRAGONv5 deterministic code has been used to perform several 2D lattice physics calculations for a possible HTR prismatic core design. The different lattice models constitute so-called SC arrangements of fuel blocks, CR blocks, and graphite blocks. These SCs were chosen based on reactor

symmetry, with the intent that the cross sections generated for a given central node (block) could be extended to all nodes in the problem that share common symmetry. Each SC consists of seven blocks (six surrounding one) and is fully heterogeneous. DRAGON solves the Boltzmann transport equation (BTE) to obtain a converged flux solution and homogenized cross sections for each assembly in a given SC. These fluxes and homogenized cross sections are then passed to the INSTANT code developed at Idaho National Laboratory. The flux computed by INSTANT is compared with the flux obtained from the lattice calculation to generate SPH correction factors that, when applied to the cross sections, preserve the reaction rates of the detailed lattice transport results. This will ultimately avoid performing a full-core heterogeneous calculation, which can take a great deal of computation time. The typical DRAGON SC calculation alone takes around 45 hours.

The DRAGON lattice code was developed at Ecole Polytechnique de Montreal [11] and is specifically versatile for the modeling of prismatic core designs associated with HTR cores. The code employs its own macro language (CLE-2000) to manage the input and execution of files according to the specific user-defined modules. It is capable of reading a variety of microscopic cross-section library formats before interpolating dilution and temperature to create a DRAGON-specific formatted library. The ENDF/B-V.II SHEM 361 energy structure is used in this work. After generation of the proper library, a geometry-tracking file is generated using the NXT module to be subsequently used in the resonance self-shielding calculation. This module is required in DRAGON when using the collision probability method in 2D hexagonal geometries. This calculation is performed on a coarse mesh representation of the SC problem. Following this, a fine mesh geometry-tracking file is generated using first the NXT module and then the MCCGT module. The addition of the latter module allows for the final solution technique to the BTE to be that of the method of characteristics. Finally, the FLU module is used to solve the linear system of equations associated with the k-eigenvalue problem.

3.1 Geometric Models

A total of five SC models were constructed as the basis for the SPHTR core. All dimensions come from the third installment of the International Criticality Safety Benchmark Evaluation Project report on the HTTR unless stated otherwise [8]. Table 3 lists the major design specifications used in the models. All SCs are composed of a central hexagon block surrounded by six additional blocks. Reflective boundary conditions are imposed on the outer boundary of the outer hexes. Figure 5 is a diagram of the full core identified by SC. The core has a central control block with three B₄C absorber rods fully inserted. Surrounding this is the innermost ring of fuel with an enrichment of 14.5%. The outer ring has 15.5% enriched fuel dispersed every other position between blocks with two B₄C absorber rods. Surrounding the outer ring are reflector blocks. Figure 6 shows the individual SCs.

Each fuel block contains 33 fuel pins. For simplicity, the centers of the fuel blocks are composed of graphite. The inner ring blocks contain two burnable poison (BP) channels on the periphery and one He channel, while the outer fuel blocks each contain one BP channel and two He channels. The TRISO fuel exists as annular compacts with He gas in the center. A uniform packing fraction of 0.30 is used for all compacts. The BIHET option is used in DRAGON to account for the double heterogeneity of these particles. The geometric mesh over the annular fuel zone is divided into six equi-cylindrical areas by use of the SPLITR function. Although this mesh was deemed acceptable by comparing a single infinite fuel block with no BPs to an identical Serpent model, it was subsequently discovered that the models were not identical. Therefore, a further spatial convergence study was performed. A similar comparison was made with the addition of BPs to both models. It was determined that a mesh consisting of five equi-cylindrical areas was sufficient over the BPs, but due to the strong depression in the local flux, the surrounding graphite mesh needed to be further refined into three equi-cylindrical areas. This leads to a difference of ~389 pcm in block eigenvalues. However, a further spatial convergence study showed that the model requires further discretization, as shown in the next section. Table 4 gives all the material number densities used in the models.

Table 3. Major geometry specifications for DRAGON SC lattice calculations.

| Dimensions | Value |
|--|-------------------------------|
| Hex block side length (cm) | 20.78461 |
| Hex block apothem (cm) | 18.0 |
| Boundary flat-to-flat (cm) | 108.0 |
| Pin pitch (cm) | 5.1 |
| Fuel pin radius (cm) | 2.05 |
| Fuel compact inner radius/outer radius (cm) | 0.5/1.3 |
| TRISO-coated fuel particle coatings radii (cm) | 0.03/0.036/0.039/0.0415/0.046 |
| BP pin radius (cm) | 0.7 |
| He channel radius (cm) | 0.75 |
| Absorber rod radius (cm) | 6.15 |

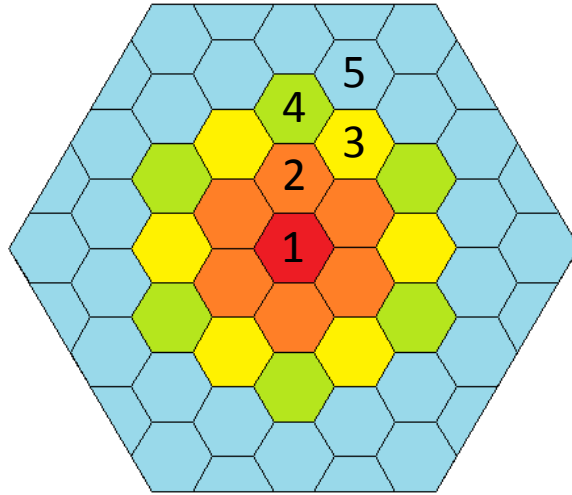


Figure 5. Full-core schematic of different SC arrangements.

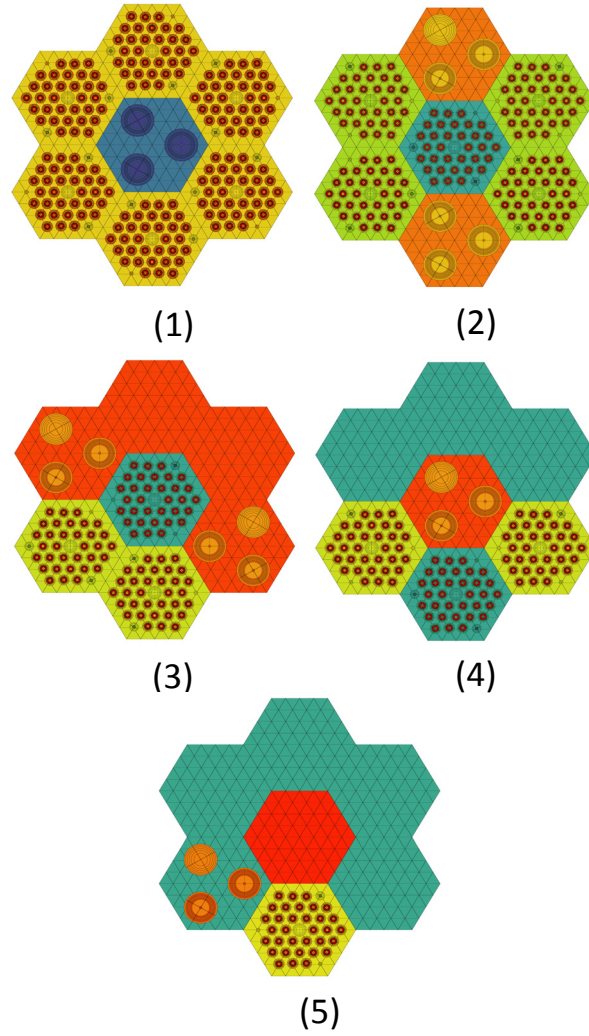


Figure 6. SC configurations, as shown in Figure 5, for generating homogeneous cross sections.

Table 4. Material number densities used in DRAGON lattice calculations.

| Material | Isotope | Number Density (atom/barn-cm) |
|---------------------------------|---------|----------------------------------|
| Graphite fuel matrix | C-graph | 8.5237E-02 |
| | B-10 | 1.5452E-08 |
| Fuel kernel (14.5 % enrichment) | U-234 | 3.5388E-05 |
| | U-235 | 3.4063E-03 |
| | U-238 | 1.9797E-02 |
| | O-16 | 4.6386E-02 |
| | O-17 | 1.7633E-05 |
| | B-10 | 1.7299E-07 |

Table 4. (continued).

| | | |
|---------------------------------|---------------------------------|------------|
| Fuel kernel (15.5 % enrichment) | U-234 | 3.5388E-05 |
| | U-235 | 3.6411E-03 |
| | U-238 | 1.9565E-02 |
| | O-16 | 4.6386E-02 |
| | O-17 | 1.7633E-05 |
| | B-10 | 1.7299E-07 |
| First TRISO porous layer | C-graph | 5.5153E-02 |
| | B-10 | 1.8290E-08 |
| Second TRISO high PyC layer | C-graph | 9.2758E-02 |
| | B-10 | 3.0761E-08 |
| Third TRISO SiC layer | C-graph | 4.8061E-02 |
| | B-10 | 5.3208E-08 |
| | Si-28 | 4.4327E-02 |
| | Si-29 | 2.2508E-03 |
| | Si-30 | 1.4837E-03 |
| Graphite sleeve | C-12 | 8.8747E-02 |
| | B-10 | 7.2596E-09 |
| He | He-3 | 3.3724E-11 |
| | He-4 | 2.4616E-05 |
| IG-110 graphite | C-12 | 8.7804E-02 |
| | B-10 | 1.1453E-08 |
| BP (2.0 wt%) | C-12 | 8.8446E-02 |
| | B-10 | 3.9906E-04 |
| | B-11 | 1.6063E-03 |
| Control rod absorber | C12 | 6.6685E-02 |
| | B-10 | 6.3184E-03 |
| | B-11 | 2.5432E-02 |
| CR clad | See Reference [8] for specifics | |

3.2 Spatial Convergence Study

The spatial convergence is performed first on a fuel pin cell and then on a fuel block due to the long running time of the SC model. Figure 7 shows the change in infinite multiplication factor (k_{inf}) as the spatial discretization increases. k_{inf} converges as the spatial discretization increases, i.e., mesh becomes finer. The converged mesh for a single fuel pin model is shown in Figure 8. The converged mesh has two, nine, and four equi-cylindrical areas for the center He, fuel matrix, and graphite sleeve, respectively, and four meshes in both X and Y Cartesian coordinates. After the converged mesh is identified for a single fuel pin, the fuel block without any BP channels is modeled using this converged mesh per fuel pin.

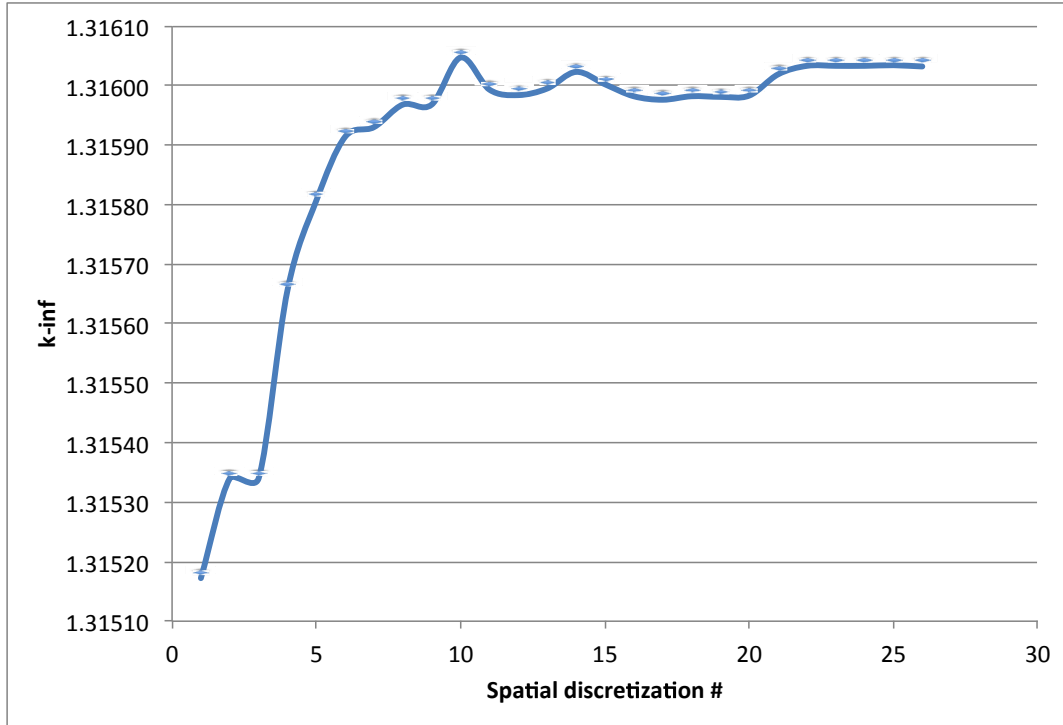


Figure 7. Dragon infinite multiplication factor (k_{inf}) versus spatial discretization for a single fuel pin.

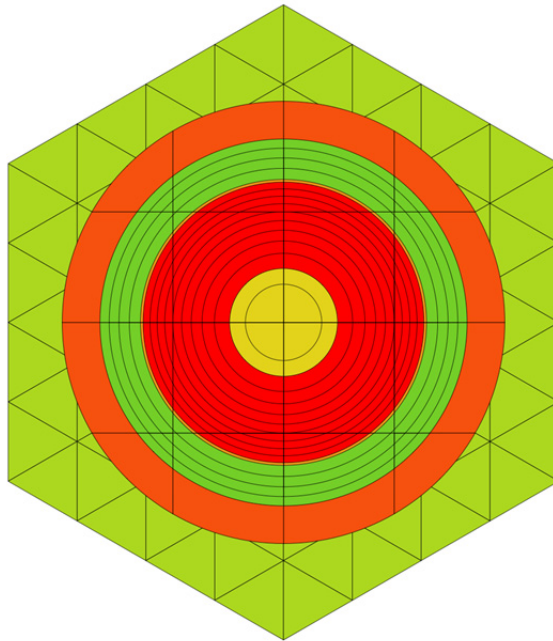


Figure 8. Converged single fuel pin mesh.

The fuel block k_{inf} as a function of spatial discretization is shown in Figure 9. The initial spatial discretizations are performed on the central tube, which was basically converged. Further discretization is then performed on the triangular mesh for the hex block. Although the triangular mesh cannot be further discretized due to an internal error message received from DRAGONv5, it can be assumed to be converged since the change is within 20 pcm. The converged mesh is shown in Figure 10. The resulting

infinite multiplication factor (k_{inf}) is 1.48360, whereas the identical Serpent model k_{inf} is 1.48443 ± 0.00003 . After the converged mesh is identified for a single fuel block without BP, the fuel block with two BP channels and a He channel is modeled using this converged mesh.

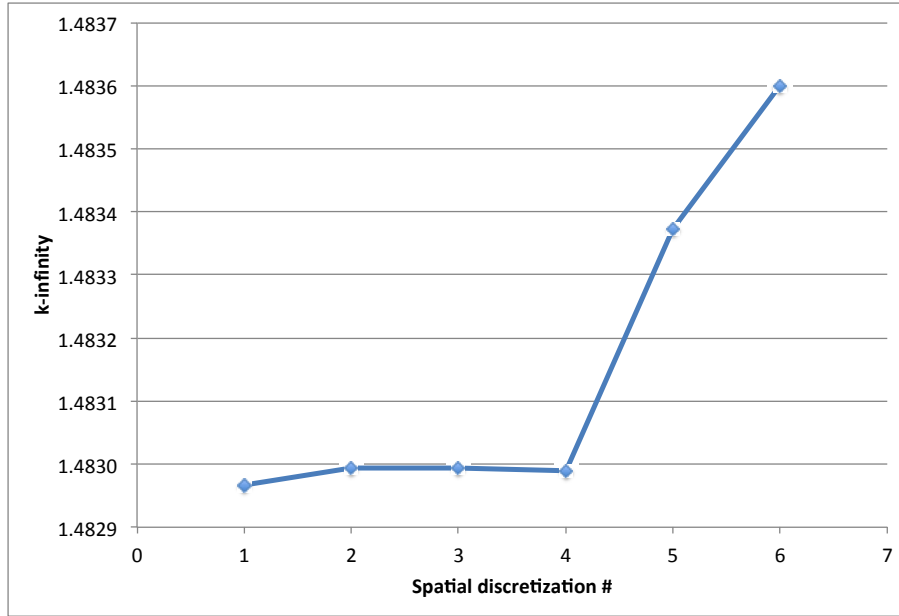


Figure 9. DRAGON k_{inf} versus spatial discretization for a fuel block without BP.

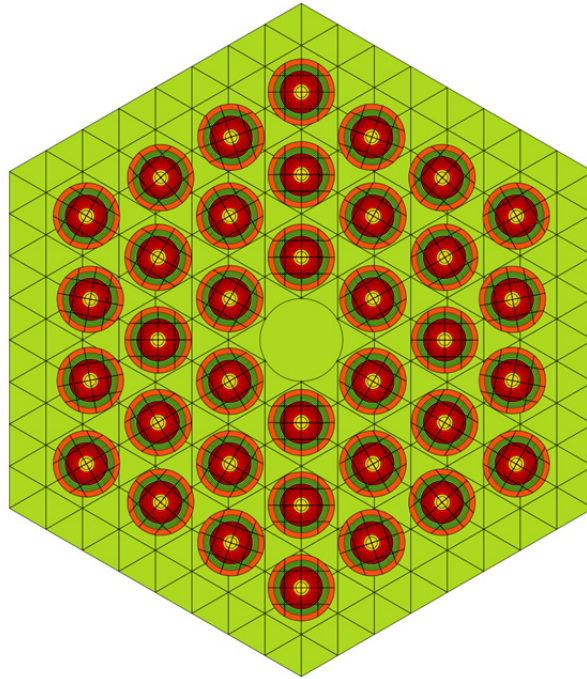


Figure 10. Converged mesh for a single fuel block without BP.

The fuel block with BP channels k_{inf} as a function of spatial discretization is shown in Figure 11. First, the BP is discretized in Cartesian coordinates; subsequently, the cylindrical discretization is performed. After the BP channel discretization is converged, further discretization of the triangular mesh for the hex

block is performed. The converged mesh is shown in Figure 12. The resulting k_{inf} is 1.36706, while the Serpent model k_{inf} is 1.36811 ± 0.00003 .

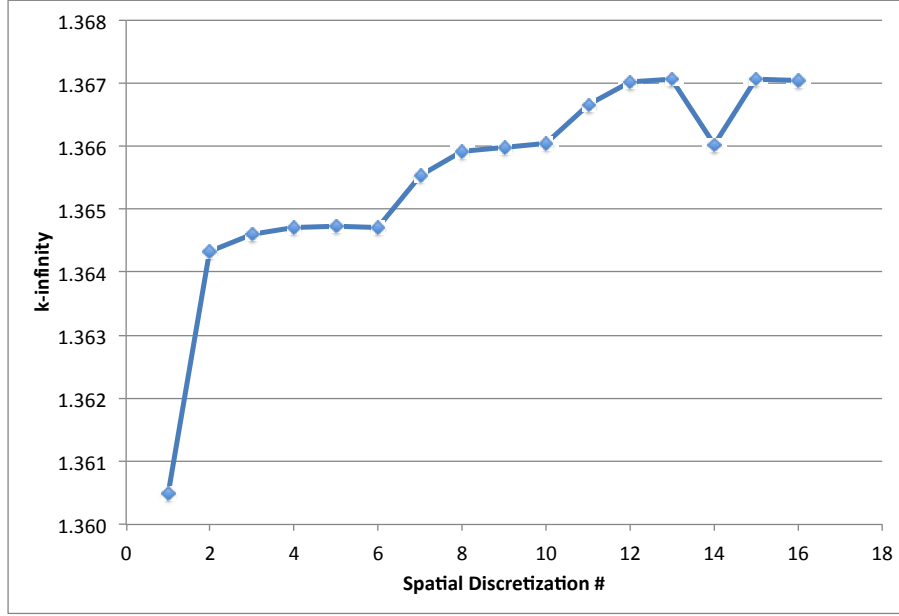


Figure 11. DRAGON k_{inf} versus spatial discretization for a fuel block with BP.

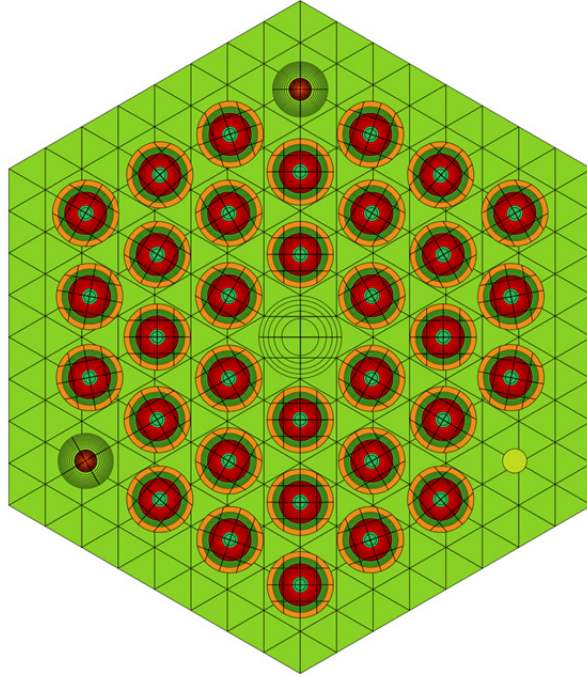


Figure 12. Converged mesh for a single fuel block with BP.

After finding the spatially converged solution for a single fuel block with BP channels, the spatial discretization of CRs is required. However, the running time of supercell models is around 45 hours. Therefore, a single fuel block with a single CR model is developed in Serpent as shown in Figure 13. The mesh without CR is already converged, k_{inf} for the Serpent model without CR is 1.42214 ± 0.0003 and

DRAGONv5 k_{inf} is 1.42056. The discretization is started with the CR channel: first the cylindrical discretization and then discretization in Cartesian coordinates is performed. The k_{inf} as a function of spatial discretization is shown in Figure 14. The final converged mesh is shown in Figure 15. The resulting k_{inf} is 0.64876 while the Serpent model k_{inf} is 0.65043 ± 0.00004 .

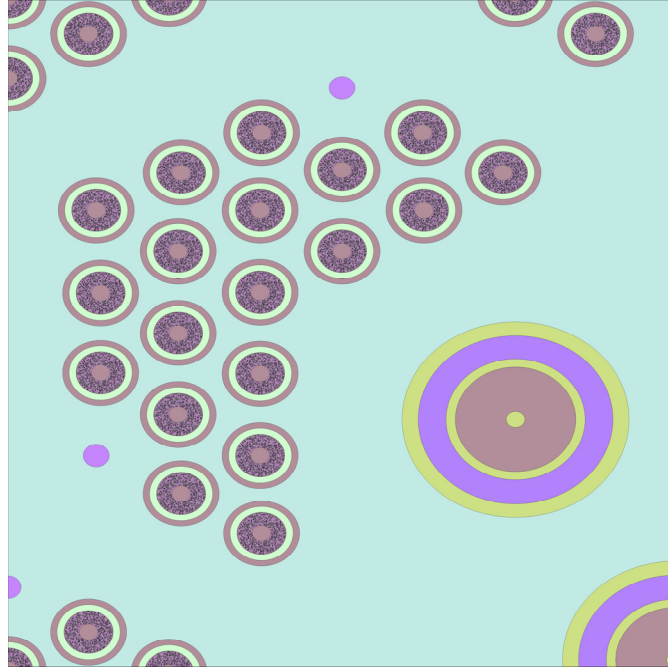


Figure 13. Serpent model of a single fuel block with BP and CR.

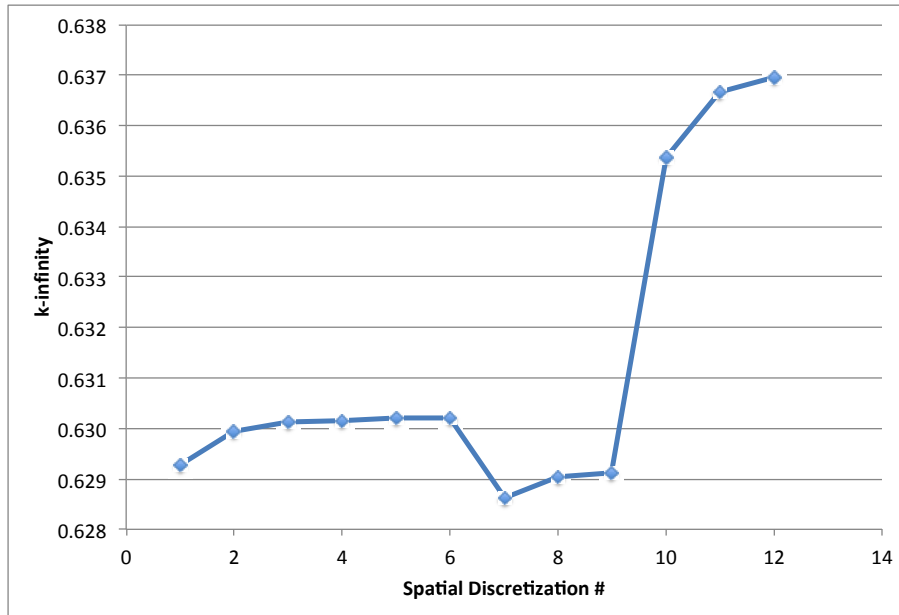


Figure 14. DRAGON k_{inf} versus spatial discretization for a fuel block with BP and CR.

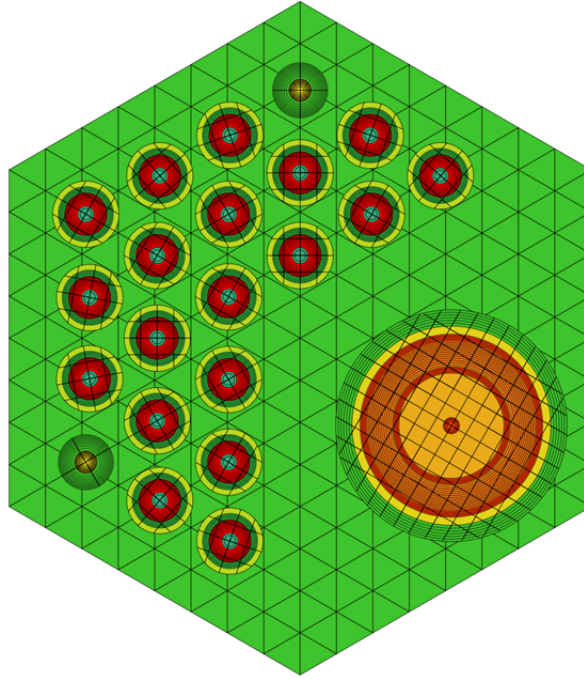


Figure 15. Converged mesh for a single fuel block with BP and CR.

3.3 DRAGON Cross-Section Generation

The simplicity in modeling hexagonal geometry along with the wide range of transport solution methodologies are a few reasons the DRAGON code was chosen as the lattice physics modeling tool for the detailed SCs to ultimately generate homogenized cross sections. The following options in DRAGON code are specifically used:

1. ANIS 2: Linearly anisotropic scattering to correct library cross sections
2. CORR: Correlated resonances of the uranium isotopes
3. IRSET 1: Intermediate resonance parameter using the statistical approximation for uranium isotopes for some energy groups
4. PT: Calculation of CALENDF-type probability tables
5. BIHET: Double heterogeneous treatment of composite TRISO fuel particles
6. NXT: Collision probability method in 2D hexagonal geometry with finite tracks (TISO)
7. NXT/MCCGT: Method of characteristics solution to the BTE.

The spatially homogenized solution is solved in 361 energy groups. For this analysis, the group structure is condensed into eight energy groups, and then the flux and cross-section solutions are passed to the INSTANT code to apply the SPH correction for further calculations. Although five SCs have been chosen for this proposed core, each was modeled with the appropriate absorber rods fully inserted and fully withdrawn, for a total of 10 heterogeneous data sets. The volume integrated fluxes and homogeneous absorption and fission reaction rates are listed in Table 5 and Table 6 for the central block of the fully rodded and unrodded cases, respectively. Table 7 lists the volume integrated 1-group fluxes and homogeneous fission and capture reaction rates for different supercells. Note that, DRAGONv5 fluxes and reaction rates are normalized to an absorption rate to be equal to one unless otherwise stated. Table 8 shows the infinite eigenvalue for each lattice model.

Table 5. DRAGON volume-integrated fluxes and homogeneous fission and absorption reaction rates of the central block for different SCs with absorber rods fully inserted.

| Energy Group | DRAGON Output | SC Central Block (Absorbers Inserted) | | | | |
|--------------|-------------------------|---------------------------------------|------------|------------|------------|------------|
| | | SC1 | SC2 | SC3 | SC4 | SC5 |
| 1 | Flux (cm/s) | 1.9627E+00 | 5.7114E+00 | 8.1618E+00 | 2.1098E+00 | 1.9899E+00 |
| | Fission (s^{-1}) | 0.0000E+00 | 7.9708E-04 | 1.2413E-03 | 0.0000E+00 | 0.0000E+00 |
| | Absorption (s^{-1}) | 6.4824E-04 | 1.1604E-03 | 1.7825E-03 | 6.1066E-04 | 6.6146E-05 |
| 2 | Flux | 7.8899E+00 | 1.4821E+01 | 1.8853E+01 | 8.3474E+00 | 8.0203E+00 |
| | Fission | 0.0000E+00 | 1.1394E-03 | 1.5659E-03 | 0.0000E+00 | 0.0000E+00 |
| | Absorption | 1.7045E-02 | 2.7212E-03 | 3.5350E-03 | 1.4706E-02 | 1.1548E-05 |
| 3 | Flux | 7.6270E+00 | 1.4907E+01 | 1.6615E+01 | 8.7721E+00 | 1.2459E+01 |
| | Fission | 0.0000E+00 | 1.2281E-02 | 1.4511E-02 | 0.0000E+00 | 0.0000E+00 |
| | Absorption | 0.0000E+00 | 2.7821E-03 | 3.8251E-03 | 0.0000E+00 | 0.0000E+00 |
| 4 | Flux | 1.1772E+00 | 3.0755E+00 | 3.3391E+00 | 1.7163E+00 | 3.9623E+00 |
| | Fission | 0.0000E+00 | 4.2141E-03 | 4.8989E-03 | 0.0000E+00 | 0.0000E+00 |
| | Absorption | 2.4917E-02 | 7.2810E-03 | 7.2759E-03 | 2.3708E-02 | 2.0732E-04 |
| 5 | Flux | 7.6795E-01 | 2.0534E+00 | 2.6369E+00 | 2.3476E+00 | 1.1048E+01 |
| | Fission | 0.0000E+00 | 9.0205E-03 | 1.2338E-02 | 0.0000E+00 | 0.0000E+00 |
| | Absorption | 1.6458E-02 | 1.2743E-02 | 1.6321E-02 | 2.4860E-02 | 1.1107E-03 |
| 6 | Flux | 9.1353E-01 | 2.3031E+00 | 3.5965E+00 | 4.6758E+00 | 2.6404E+01 |
| | Fission | 0.0000E+00 | 1.4428E-02 | 2.3015E-02 | 0.0000E+00 | 0.0000E+00 |
| | Absorption | 1.9713E-02 | 2.0525E-02 | 3.1486E-02 | 4.3771E-02 | 3.6943E-03 |
| 7 | Flux | 7.5967E-01 | 1.8191E+00 | 3.1344E+00 | 4.7874E+00 | 2.8365E+01 |
| | Fission | 0.0000E+00 | 1.5684E-02 | 2.7334E-02 | 0.0000E+00 | 0.0000E+00 |
| | Absorption | 1.6753E-02 | 2.1386E-02 | 3.6243E-02 | 4.3994E-02 | 5.7380E-03 |
| 8 | Flux | 2.8023E-01 | 6.1049E-01 | 1.1210E+00 | 2.0037E+00 | 1.2194E+01 |
| | Fission | 0.0000E+00 | 9.1871E-03 | 1.6723E-02 | 0.0000E+00 | 0.0000E+00 |
| | Absorption | 6.4071E-03 | 1.2174E-02 | 2.1806E-02 | 1.8690E-02 | 4.4212E-03 |

Table 6. DRAGON volume-integrated fluxes and homogeneous fission and absorption reaction rates of the central block for different SCs with absorber rods fully withdrawn.

| Energy Group | DRAGON Output | SC Central Block (Absorbers Withdrawn) | | | | |
|--------------|-------------------------|--|------------|------------|------------|------------|
| | | SC1 | SC2 | SC3 | SC4 | SC5 |
| 1 | Flux (cm/s) | 2.8381E+00 | 6.8573E+00 | 1.1348E+01 | 3.1030E+00 | 2.3062E+00 |
| | Fission (s^{-1}) | 0.0000E+00 | 9.7986E-04 | 1.7799E-03 | 0.0000E+00 | 0.0000E+00 |
| | Absorption (s^{-1}) | 6.3680E-05 | 1.4174E-03 | 2.5405E-03 | 7.0311E-05 | 7.4670E-05 |
| 2 | Flux | 1.0720E+01 | 1.7010E+01 | 2.4389E+01 | 1.1374E+01 | 9.0448E+00 |
| | Fission | 0.0000E+00 | 1.3115E-03 | 2.0363E-03 | 0.0000E+00 | 0.0000E+00 |
| | Absorption | 1.9968E-06 | 3.1103E-03 | 4.5599E-03 | 2.1011E-06 | 2.5332E-06 |
| 3 | Flux | 1.5717E+01 | 1.6976E+01 | 2.0173E+01 | 1.6113E+01 | 1.4189E+01 |
| | Fission | 0.0000E+00 | 1.4068E-02 | 1.7634E-02 | 0.0000E+00 | 0.0000E+00 |
| | Absorption | 8.1338E-05 | 5.2277E-02 | 6.1611E-02 | 8.3447E-05 | 1.1103E-04 |
| 4 | Flux | 4.4824E+00 | 3.9394E+00 | 4.4698E+00 | 4.8311E+00 | 5.0119E+00 |
| | Fission | 0.0000E+00 | 5.3797E-03 | 6.5454E-03 | 0.0000E+00 | 0.0000E+00 |
| | Absorption | 1.3978E-04 | 9.2126E-03 | 9.7502E-03 | 1.5265E-04 | 2.3860E-04 |
| 5 | Flux | 4.1982E+00 | 3.5333E+00 | 5.6589E+00 | 9.0778E+00 | 2.0858E+01 |
| | Fission | 0.0000E+00 | 1.5490E-02 | 2.6474E-02 | 0.0000E+00 | 0.0000E+00 |
| | Absorption | 2.5007E-04 | 2.1789E-02 | 3.5244E-02 | 5.5307E-04 | 1.8846E-03 |
| 6 | Flux | 6.4248E+00 | 5.1319E+00 | 1.0331E+01 | 1.9712E+01 | 5.2779E+01 |
| | Fission | 0.0000E+00 | 3.0735E-02 | 6.3272E-02 | 0.0000E+00 | 0.0000E+00 |
| | Absorption | 5.4345E-04 | 4.3570E-02 | 8.6277E-02 | 1.6807E-03 | 6.6104E-03 |
| 7 | Flux | 5.9840E+00 | 4.5581E+00 | 9.9643E+00 | 2.0651E+01 | 5.7430E+01 |
| | Fission | 0.0000E+00 | 3.7481E-02 | 8.3483E-02 | 0.0000E+00 | 0.0000E+00 |
| | Absorption | 7.3206E-04 | 5.0922E-02 | 1.0981E-01 | 2.5427E-03 | 1.0379E-02 |
| 8 | Flux | 2.3834E+00 | 1.6426E+00 | 3.7638E+00 | 8.7599E+00 | 2.4831E+01 |
| | Fission | 0.0000E+00 | 2.3359E-02 | 5.3741E-02 | 0.0000E+00 | 0.0000E+00 |
| | Absorption | 5.1980E-04 | 3.0865E-02 | 6.9462E-02 | 1.9238E-03 | 8.0058E-03 |

Table 7. Volume integrated fluxes and homogeneous fission and absorption reaction rates of the central block in 1 energy group for different SCs with absorber rods fully withdrawn

| Energy Group | DRAGON Output | Supercell Central Block (Absorbers OUT) | | | | |
|--------------|-------------------------|---|------------|------------|------------|------------|
| | | SC1 | SC2 | SC3 | SC4 | SC5 |
| 1 | Flux (cm/s) | 5.2747E+01 | 5.9648E+01 | 9.0097E+01 | 9.3622E+01 | 1.8645E+02 |
| | Fission (s^{-1}) | 0.0000E+00 | 1.2880E-01 | 2.5497E-01 | 0.0000E+00 | 0.0000E+00 |
| | Absorption (s^{-1}) | 2.3322E-03 | 2.1316E-01 | 3.7926E-01 | 7.0089E-03 | 2.7307E-02 |

Table 8. Infinite multiplication factors for heterogeneous DRAGON SC calculations.

| Heterogeneous SC | k-infinity |
|------------------|------------|
| SC 1 (rods in) | 1.0639090 |
| SC 2 (rods in) | 0.9814761 |
| SC 3 (rods in) | 0.8851578 |
| SC 4 (rods in) | 1.0045930 |
| SC 5 (rods in) | 0.8770997 |
| SC 1 (rods out) | 1.3926180 |
| SC 2 (rods out) | 1.4810420 |
| SC 3 (rods out) | 1.4675740 |
| SC 4 (rods out) | 1.4473350 |
| SC 5 (rods out) | 1.3407840 |

4. HTR FULL-CORE SIMULATION APPLYING SPH METHOD

The HTR core remains highly heterogeneous even after each block is homogenized for use in the full-core calculations because of the differences in properties of fuel blocks (enrichment, burnup, presence of BPs, etc.). Therefore, the full-core calculations still need to capture such large-scale heterogeneous effects in order to preserve the local reaction rates and leakages. A tremendous number of studies have been performed to improve the accuracy of full-core calculations through the homogenization procedure [12]. However, those studies were mostly performed for light-water reactor analyses; thus, the studies may not be directly applicable to advanced thermal reactors such as HTRs. This section of the report presents the preliminary study of the HTR full-core calculations utilizing the SPH method.

The SPH method was first introduced by Kavenoky in the early 1980s [13]. Later, Hébert established a more theoretical basis of the equivalence relation for the SPH method and applied it to pin-by-pin and assembly-homogenization procedures [14,15] for pressurized-water reactors. This method attempts to preserve the balanced relations (reaction rates, leakage, etc.) over a given *macroregion* by multiplying SPH equivalence factors to cross sections belonging to a given *macroregion* and energy group. Here, the *macroregion* refers to the collection of fuel pins or assemblies that well represent part of or the whole-core geometry. An SC geometry could be seen as equivalent to the *macroregion*. The overall performance of the SPH method is determined by how efficiently it calculates the SPH equivalence factors, μ_i^g , that can reproduce the reaction rates, which is given by:

$$\mu_i^{g,(l+1)} = \frac{\bar{\Phi}_{Het,i}^g}{\bar{\Phi}_{Hom,i}^{g,(l)}}, \quad \text{for } i = 1, \dots, I, g = 1, \dots, G \quad (1)$$

where $\bar{\Phi}_{Het,i}^g$ and $\bar{\Phi}_{Hom,i}^{g,(l)}$ correspond to average heterogeneous and homogeneous group g scalar fluxes over the i^{th} region, respectively. The heterogeneous flux refers to the flux calculated by lattice physics burnup calculations, whereas the homogeneous flux refers to the flux from the coarse-mesh calculations commonly performed by nodal-diffusion or transport codes. This calculated SPH factor is multiplied by the homogenized multigroup cross sections calculated by the lattice physics code:

$$\hat{\Sigma}_i^{g,(l)} = \mu_i^{g,(l)} \cdot \Sigma_i^g, \quad \text{for } i = 1, \dots, I, g = 1, \dots, G. \quad (2)$$

Since the calculation of the SPH factors uses homogeneous fluxes that are not guaranteed to reproduce the reaction rates of the detailed heterogeneous models, it is necessary to adjust the cross sections iteratively until the reaction rates produced by the homogeneous model converge to an acceptable

approximation of the higher fidelity result. Furthermore, the value of the calculated SPH factor highly depends on the type of discretization methods used for the calculation of homogeneous fluxes. Figure 16 illustrates one of proposed procedures that is considered being an effective, albeit conservative, process to calculate and use the SPH factors for the full-core calculations. In this procedure, the HTR core to be modeled is assumed to consist of several macroregions, each of which can be modeled as a separate SC. Imposing reflective boundary conditions at the outer surfaces of these SC, the lattice physics calculations are performed to obtain homogenized and collapsed cross sections and heterogeneous average group fluxes (step a). By utilizing the homogenized cross sections, the homogeneous fluxes are calculated for the homogenized macroregion modeled by the nodal (or coarse mesh) code that will be used for the actual full-core calculations (step b). After that, the SPH factors are calculated by *Equation (1)* (step c). Steps (b) and (c) are repeated using *Equations (1)* and (2) until all SPH factors are sufficiently converged. Finally, in step (d), the full-core calculation is performed using converged SPH factors and homogenized cross sections. This process is illustrated in Figure 16.

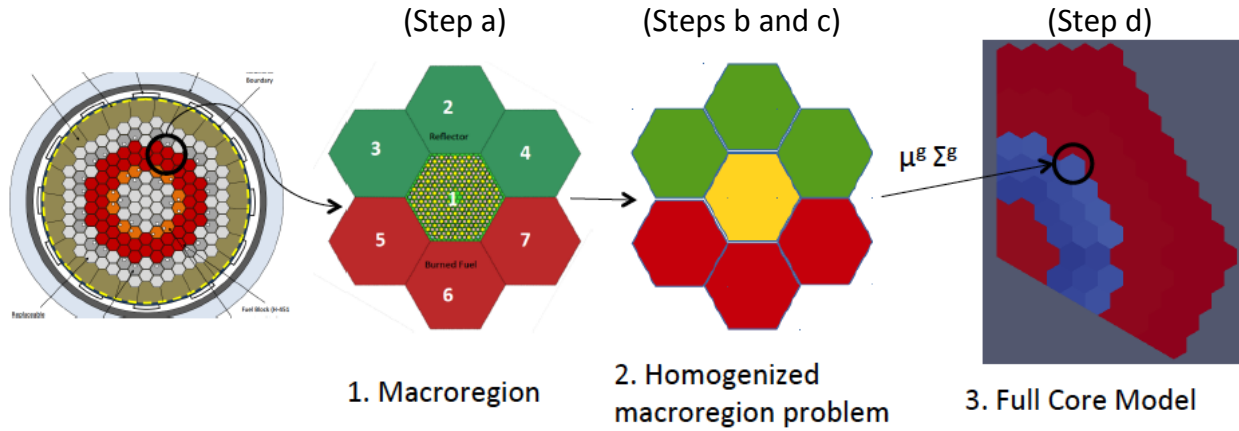


Figure 16. The proposed SPH process for the HTR full-core calculations.

Although the SPH method used here has a strong equivalence relation to the local average reaction rates, there is a weak relation preserving interface currents, unlike the Generalized Equivalence Theory [12], which imposes a discontinuity of interface fluxes in order to provide a degree of freedom to the coarse-mesh nodal calculations for preserving interface currents. Additional effort, which is beyond the scope of this report, may be necessary preserve interface currents in the SPH procedure described in this report.

4.1 SPH Test Problem Performed with a Seven-Node HTR Supercell Model

In order to perform simple exercises for the SPH method, a 2D, seven-node, modular HTR gas-cooled reactor SC INSTANT model was constructed, as shown in Figure 17. This SC model consists of one heterogeneous fuel block located at the center surrounded by six smeared blocks, three of which are burned fuel blocks and the rest are graphite reflector blocks. The details of the dimensions and fuel properties can be found in the reference [16]. The lattice physics burnup code HELIOS-2 was used for generating self-shielded homogenized eight-group cross sections. The energy group's lower boundaries for the eight-group structure are listed in Table 9. The calculation of the homogeneous flux over each block was performed by the INSTANT module in the Idaho National Laboratory's PHISICS code system [17], which can solve the second-order P_N equations by means of the variational nodal method over the 2D/3D Cartesian and hexagonal nodes (Figure 17). The HELIOS-2 model also includes six

diamond-shaped void nodes at the outer edges, which create six outer boundary surfaces surrounding this SC model. The reflective boundary conditions were imposed on these six surfaces in the HELIOS-2 model while the same conditions were applied to outer surfaces of surrounding hexagonal nodes in the INSTANT model. Note that, HELIOS-2 code is used for the simple test model since the SPH iteration interface was already build between HELIOS-2 and INSTANT codes.

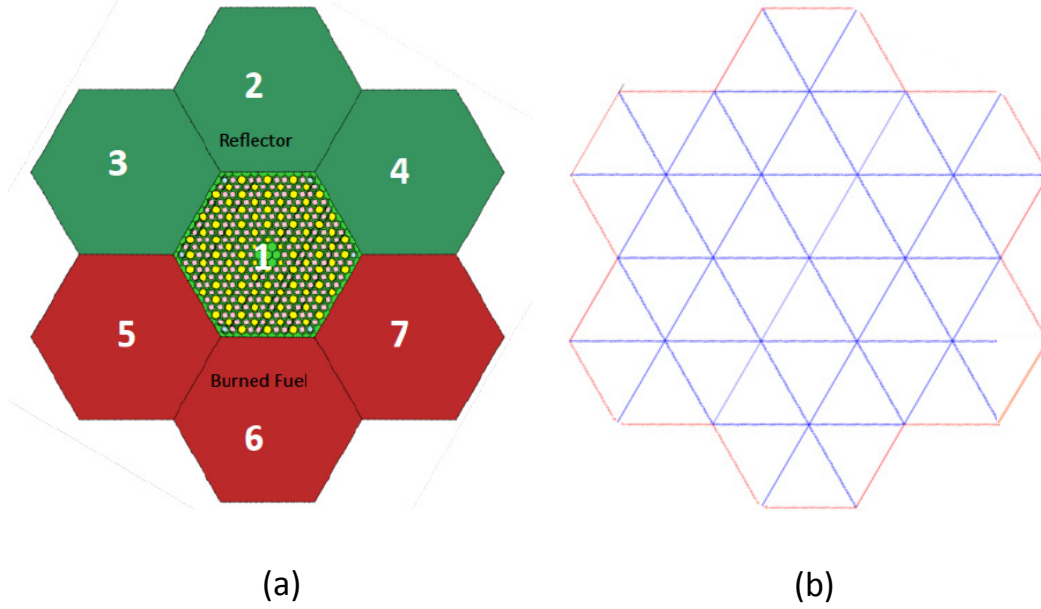


Figure 17. Seven-node modular HTTr gas-cooled reactor SC model: (a) HELIOS-2 model and (b) INSTANT model.

Table 9. Lower energy boundaries for the eight-group structure.

| Energy Group | Lower Energy Boundary [eV] |
|--------------|----------------------------|
| 1 | 2.2313E+06 |
| 2 | 8.2085E+05 |
| 3 | 4.8810E+03 |
| 4 | 1.3007E+02 |
| 5 | 3.9279E+00 |
| 6 | 6.2506E-01 |
| 7 | 1.4572E-01 |
| 8 | 0.0000E+00 |

The first study was performed to investigate the behavior of eigenvalue (k_{inf}) and reaction rates during iterations to find converged SPH factors, μ_i^g , utilizing *Equations (1) and (2)*. Figure 18 shows the convergence behavior of the eigenvalue during the SPH factor iterations. The convergence behaviors of the absorption and fission reaction rates are presented in Figure 19. Both eigenvalue and reaction rates rapidly approach the HELIOS-2 reference solutions during the first 15 iterations and then gradually reach stable values that are close to the reference solutions. However, these solutions did not exactly reach the reference solutions because of the differences in the interface currents and the outer boundaries between two models. Similar behavior can be observed in the convergence behavior of the SPH equivalence factor shown in Figure 20. In most of the energy groups the SPH factors converge to values ranging from 0.8 to 1.8.

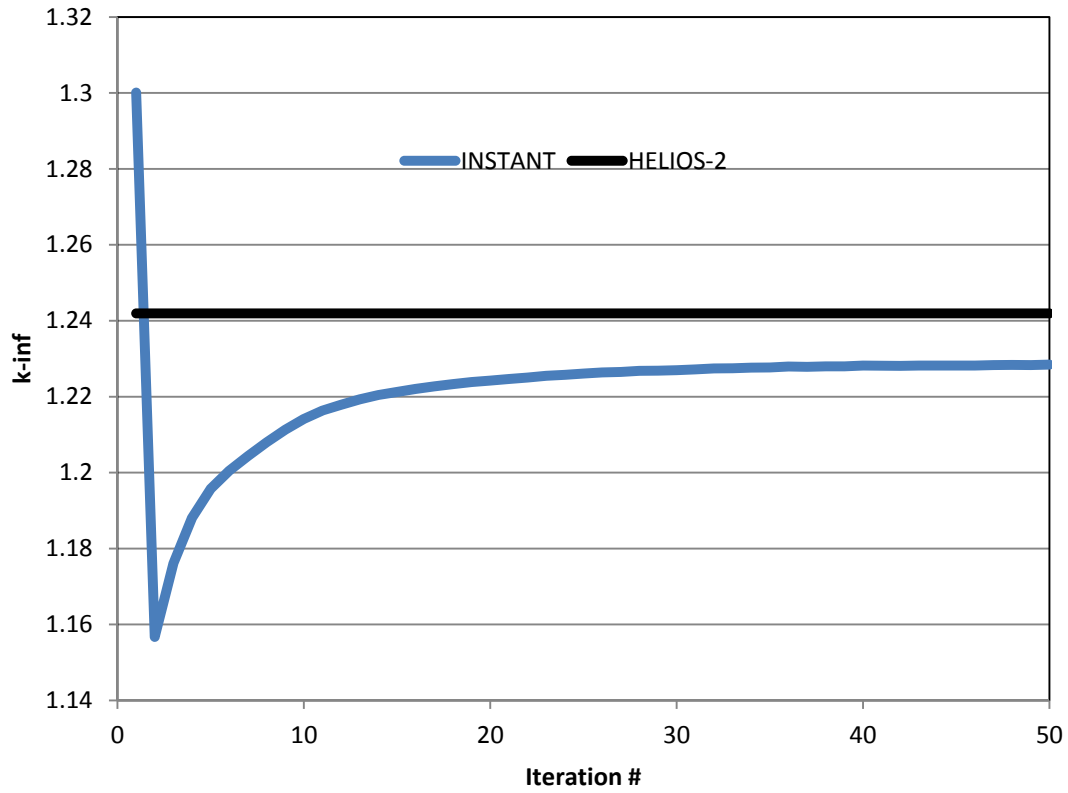


Figure 18. Eigenvalue convergence behavior during the SPH factor iteration.

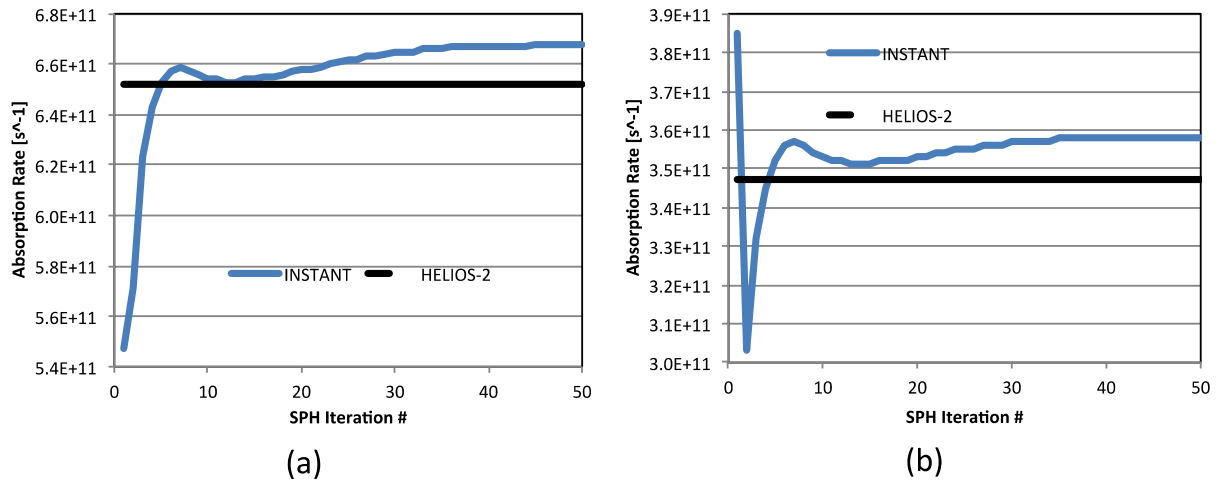


Figure 19. Reaction rates convergence behavior during the SPH factor iteration: (a) absorption rate and (b) fission rate.

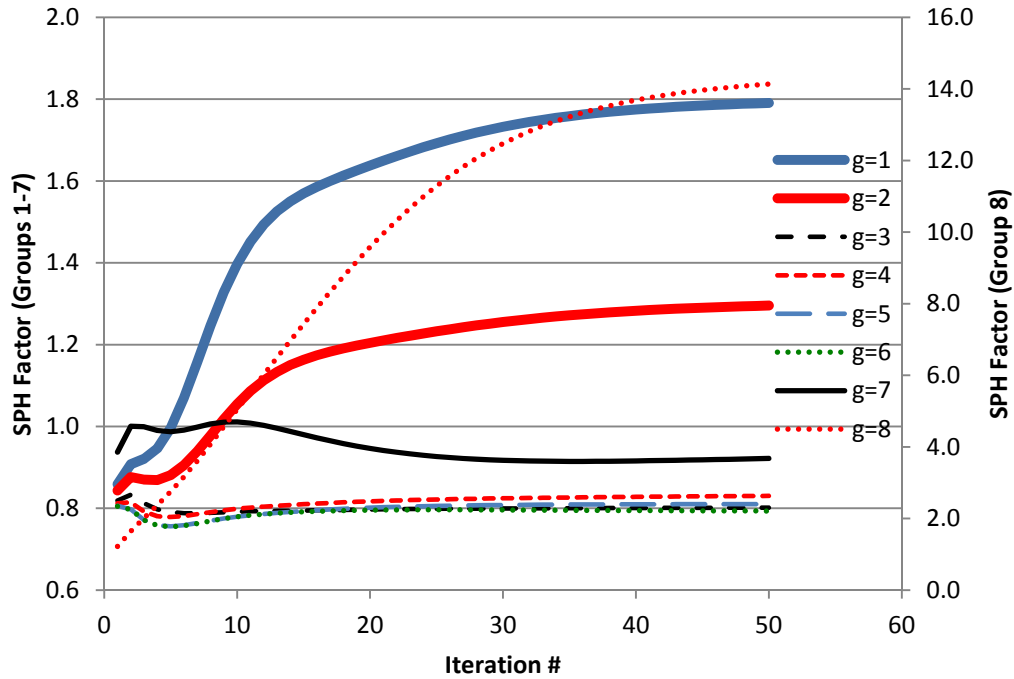


Figure 20. Convergence behavior of SPH equivalence factors.

The converged SPH factors were used for the seven-node test problems in order to determine whether the local reaction rates can be reproduced. The process is summarized in Figure 21. The converged SPH factors were already obtained, corresponding to Step 3 in this figure. In the final step (Step 4), only the SPH factors of the central node are provided to the seven-node problem while the surrounding nodes use an uncorrected set of cross sections generated by HELIOS-2 in Step 1. Table 10 compares absorption and fission reaction rates in the central node calculated with and without SPH corrections. The reaction rates with the SPH correction in this process were almost exactly reproduced, despite the fact that the reaction rates did not converge exactly during the SPH factor iteration, as seen in Table 10. This is promising for full-core calculations with SPH corrections if the heterogeneous SC model can accurately represent local phenomena.

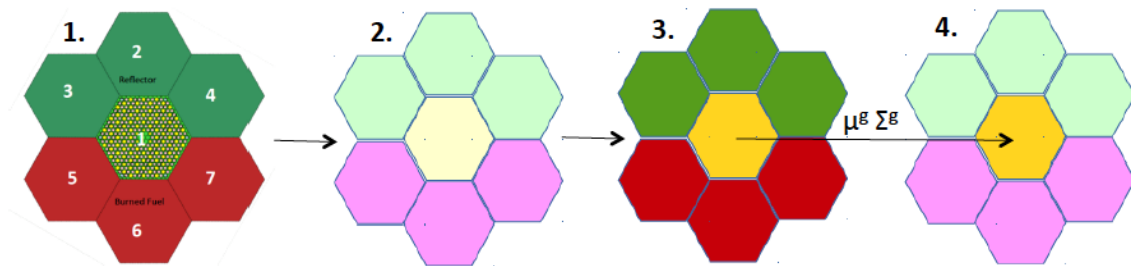


Figure 21. The process for the seven-node test problem with SPH corrections.

Table 10. Comparison of reaction rates calculated with and without SPH corrections.

| Code | Absorption Rate [$\times 10^{11} \text{ sec}^{-1}$] | Fission Rate [$\times 10^{11} \text{ sec}^{-1}$] |
|---------------------|---|--|
| HELIOS-2 | 6.515 | 3.471 |
| INSTANT with SPH | 6.435 | 3.470 |
| INSTANT without SPH | 5.473 | 3.848 |

4.2 Preliminary Results for the Simplified Full-Core HTR Calculations with SPH Procedure

The SPH exercise for the HTR model was extended to the 2D mini full-core model, which was named SPHTR. As explained in the analysis of the lattice-physics SC models presented in Section 3, this mini full-core model consists of five unique SC models, each of which includes one or two control blocks. The resulting core includes five different blocks, which are the inner and outer fuel blocks, central and outer CRs, and graphite reflector blocks, as shown in Figure 22. The vacuum boundary conditions were imposed on all outer graphite block surfaces. As presented in Subsection 3.3, homogenized eight-group cross sections, whose energy boundaries correspond to those in Table 9, were generated by the DRAGONv5 lattice physics code using SC models.

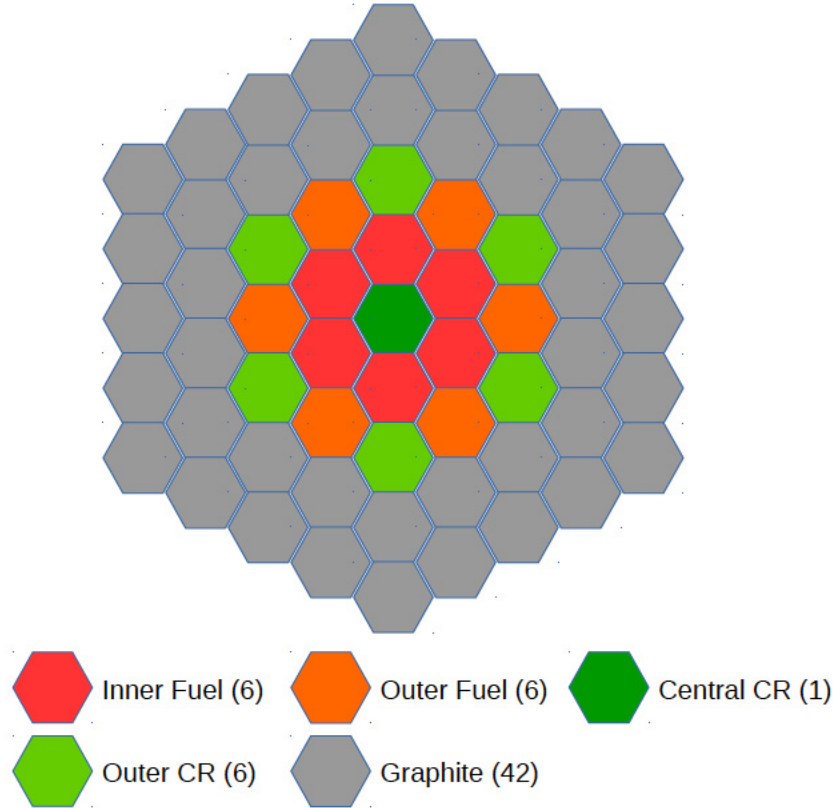


Figure 22. The simplified 2D HTR test geometry (SPHTR).

Following the procedure given in the beginning of this section—i.e., *Equations (1) and (2)* and Figure 16—the SPH correction factors were generated for the central node of each SC. The results of each SC model (k_{inf} , absorption and fission rates) after 50 SPH iterations are summarized in Table 11 and Table 12. Originally the method was proposed to perform SPH corrections for all 7 nodes. This originally proposed approach provided excellent agreement between DRAGON and INSTANT results for most of SCs, except for SC 2 in rodded cases, which failed to converge by the proposed method. In all rodded SC

cases severe decreases in heterogeneous group fluxes were observed within these nodes; nodal codes typically cannot capture such decreases without extra interface treatments. The large difference between heterogeneous and calculated homogeneous fluxes resulted in considerably large SPH factors, which made solutions difficult to converge. Therefore, SPH iterations for the rodged SC 2 were applied to only central nodes. This modified approach still provided converged SPH factors and close agreement in reaction rates.

Table 11. Comparison of INSTANT and DRAGON results for each rodged SC.

| | K_{inf} | | Absorption Rate* [s ⁻¹] | | Fission Rate* [s ⁻¹] | |
|---|-----------|-----------|-------------------------------------|------------|----------------------------------|------------|
| | INSTANT | DRAGON | INSTANT | DRAGON | INSTANT | DRAGON |
| SC 1 | 1.0639283 | 1.0639090 | 2.0896E-01 | 2.0871E-01 | N/A | N/A |
| SC 2** | 1.0197171 | 0.9814761 | 1.2437E-01 | 1.2340E-01 | 6.7362E-02 | 6.6751E-02 |
| SC 3 | 0.8849793 | 0.8851578 | 1.6911E-01 | 1.6894E-01 | 1.0172E-01 | 1.0163E-01 |
| SC 4 | 1.0044174 | 1.0045930 | 2.6215E-01 | 2.6192E-01 | N/A | N/A |
| SC 5 | 0.8781305 | 0.8770997 | 1.5328E-02 | 1.5361E-02 | N/A | N/A |
| *Normalized reaction rates. | | | | | | |
| **SPH applied only on the central node. | | | | | | |

Table 12. Comparison of INSTANT and DRAGON results for each unrodged SC.

| | k_{inf} | | Absorption Rate* [s ⁻¹] | | Fission Rate* [s ⁻¹] | |
|-----------------------------|-----------|-----------|-------------------------------------|------------|----------------------------------|------------|
| | INSTANT | DRAGON | INSTANT | DRAGON | INSTANT | DRAGON |
| SC 1 | 1.3925604 | 1.3926180 | 2.3360E-03 | 2.3381E-03 | N/A | N/A |
| SC 2 | 1.4810231 | 1.4810420 | 2.1334E-01 | 2.1316E-01 | 1.2891E-01 | 1.2880E-01 |
| SC 3 | 1.4675017 | 1.4675740 | 3.7947E-01 | 3.7926E-01 | 2.5510E-01 | 2.5497E-01 |
| SC 4 | 1.4469221 | 1.4473350 | 7.0131E-03 | 7.0159E-03 | N/A | N/A |
| SC 5 | 1.3406050 | 1.3407840 | 2.7314E-02 | 2.7295E-02 | N/A | N/A |
| *Normalized reaction rates. | | | | | | |

Table 13 shows k_{eff} results for the unrodged case calculated without SPH corrections, with SPH corrections for all nodes and selected nodes (fuel and CR nodes or only fuel nodes), along with the reference Serpent result. The cross sections and fluxes used in the SPH calculations are all from the unrodged supercell calculations, shown in Table 11. The INSTANT full-core calculation without SPH correction eigenvalue is about 1.26, which is 2,000 pcm larger than the reference Serpent 2D calculation. When the SPH correction is applied to all nodes, k_{eff} was slightly decreased, approximately 250 pcm lower than the case without SPH correction. Applying SPH correction to selected nodes did not improve the eigenvalue result.

Table 13. Comparison of k_{eff} in the unrodged case.

| Type of Methods | k_{eff} |
|---|-------------------|
| INSTANT without SPH | 1.26405 |
| INSTANT with SPH (all nodes) | 1.26152 |
| INSTANT with SPH (fuel and CR nodes only) | 1.26613 |
| INSTANT with SPH (fuel nodes only) | 1.27066 |
| Serpent (2D Model CR out) | 1.24569 ± 0.00002 |

Table 14 shows k_{eff} results for the case with rods inserted, calculated without SPH corrections, with SPH corrections for all nodes, and with SPH corrections for only CR nodes, along with the reference Serpent result. As seen in this table, k_{eff} of the INSTANT full-core calculation without SPH correction was 0.73, which is about 2,500 pcm lower than the Serpent 2D model result. Applying SPH corrections to all nodes and only CR nodes further decreased k_{eff} , approximately 1,000 and 2,000 pcm lower than the case without SPH correction, respectively.

At this moment, comparing results in Table 13 and Table 14, the SPH method does not have significant impact on the k_{eff} results. However, note that the DRAGONv5 supercell calculations are not spatially converged as mentioned in section 3. The DRAGONv5 and Serpent SC-1 model k_{eff} results for the rodged case are 1.06391 and 1.18726 ± 0.0005 , respectively, i.e. the difference is about 12000 pcm. The difference in the unrodged case is about 1000 pcm. The supercell calculations are also compared with void boundary conditions, since using the reflective boundary conditions generates slightly different models. In that case, the DRAGONv5 k_{eff} for SC 1 is 0.20704, whereas the Serpent k_{eff} is 0.23952 ± 0.0002 , still more than about 3000 pcm difference.

Table 14. Comparison of k_{eff} in the rodged case.

| Type of Methods | k_{eff} |
|-------------------------------------|-----------------------|
| INSTANT without SPH | 0.731020 |
| INSTANT with SPH (all nodes) | 0.712640 |
| INSTANT with SPH (only CR nodes) | 0.723274 |
| Serpent (2D model with CR inserted) | 0.75560 ± 0.00004 |

The comparison of absorption and fission reaction rates per node defined by each supercell is given Table 15 for the unrodged case. Both fission and absorption reaction rates when the two codes compared show better agreement, about 2% relative difference, for the inner fuel and outer fuel nodes. However, the absorption rate for the central and outer CR nodes shows large differences, 20% and 80%, respectively. A better agreement between the INSTANT and Serpent full-core models could be obtained by generating transport corrected reflector cross sections in order to accurately take into account the neutron leakage from the core.

The overall results could improve by using spatially converged lattice physics models for the SPH correction iteration or by generating transport corrected cross sections for the graphite reflector blocks. However, the effect of SPH correction might stay the same. Since as mentioned earlier, currently the INSTANT code does not have a capability of using discontinuity factors. As a result, in the current framework of SPH corrections mentioned in this report, all leakage (or interface current) corrections are included in the SPH correction factors, which could produce unphysically large cross sections due to the large heterogeneous flux tilts caused by absorbers. The further improvement is necessary in order to preserve the interface current separately from the SPH correction.

Table 15. Comparison of INSTANT and Serpent reaction rates in 2D full-core models with control rods withdrawn.

| Code | Reaction Rate (s^{-1}) | Inner Fuel | Outer Fuel | Central CR | Outer CR |
|-----------------|----------------------------|------------|------------|------------|------------|
| Serpent (2D) | Absorption | 4.8839E+16 | 4.4821E+16 | 8.7238E+14 | 9.2439E+14 |
| | Fission | 2.8610E+16 | 2.8965E+16 | 0.0000E+00 | 0.0000E+00 |
| INSTANT w/o SPH | Absorption | 4.7969E+16 | 4.5315E+16 | 6.9591E+14 | 1.8456E+14 |
| | Fission | 2.8254E+16 | 2.9359E+16 | 0.0000E+00 | 0.0000E+00 |

Table 15. (continued).

| Code | Reaction Rate (s^{-1}) | Inner Fuel | Outer Fuel | Central CR | Outer CR |
|-------------------------------|----------------------------|------------|------------|------------|------------|
| INSTANT w/ SPH (All nodes) | Absorption | 4.7504E+16 | 4.5599E+16 | 6.6781E+14 | 1.6869E+14 |
| | Fission | 2.8001E+16 | 2.9612E+16 | 0.0000E+00 | 0.0000E+00 |
| INSTANT w/ SPH (Fuel & CR) | Absorption | 4.7439E+16 | 4.5726E+16 | 6.6524E+14 | 1.8476E+14 |
| | Fission | 2.7968E+16 | 2.9646E+16 | 0.0000E+00 | 0.0000E+00 |
| INSTANT w/ SPH (Fuel only) | Absorption | 4.7674E+16 | 4.5530E+16 | 6.7189E+14 | 1.7947E+14 |
| | Fission | 2.8111E+16 | 2.9502E+16 | 0.0000E+00 | 0.0000E+00 |

5. CONCLUSIONS

A hypothetical prismatic HTR core is modeled with Serpent Monte Carlo code as the reference calculation to validate the homogenized group constant generation methodology used in the report. All the models generated with DRAGONv5 for the lattice physics calculations were compared with a respective Serpent model. The spatial convergence of the lattice physics code models was also investigated. After spatially convergence was ensured, all the DRAGONv5 results compared to the eigenvalue Serpent results well. The differences in infinite medium eigenvalues were less than 200 pcm.

The results showed that the spatial convergence of the deterministic calculations is important, especially when local strong absorbers are present. The local depression in the flux requires finer meshing, which increases runtime. Although the group constants can be generated with a full-core Serpent calculation for the isothermal 2D SPHTR model with a practical runtime, this is not always practical for a non-symmetric full-size reactor with non-uniform temperature profiles.

The impact of the SPH correction on the full-core eigenvalue results was very small in both rodged and unrodged cases. This is partially due to fairly close eigenvalue results obtained even without SPH correction on the INSTANT. However, further improvement can be expected if the method to preserve interface currents is implemented in the current procedure. A better agreement between INSTANT and Serpent full-core model results could also be obtained by generating transport corrected reflector cross sections in order to accurately take into account the neutron leakage from the core.

6. REFERENCES

-
- [1] Leppänen, J., et al., “The Serpent Monte Carlo code: Status, development and applications in 2013.” *Annals of Nuclear Energy*, Vol. 82, 2015. pp. 142-150.
 - [2] Leppanen, J., M. Pusa, and E. Fridman, “Overview of methodology for spatial homogenization in the Serpent 2 Monte Carlo Code,” *Annals of Nuclear Energy*, Vol. 96, 2016, pp. 126–136.
 - [3] Koebke, K., *A new approach to homogenization and group condensation*, IAEA-TECDOC-231, International Atomic Energy Agency, 1978.
 - [4] Smith, K., *Spatial Homogenization Methods for Light Water Reactor Analysis*, Ph.D. Thesis: Massachusetts Institute of Technology, Cambridge, Massachusetts, 1980.
 - [5] Bell, G.I. and S. Glasstone, *Nuclear Reactor Theory*, New York: Van Nostrand Reinhold Company, 1970.

-
- [6] Duderstadt, J. J. and L. J. Hamilton, *Nuclear Reactor Analysis*, Hoboken: John Wiley & Sons, Inc., 1976.
- [7] Stamm'ler, R. and M. Abbate, *Methods of Steady-State Reactor Physics in Nuclear Design*, Cambridge: Academic Press, Inc., 1983.
- [8] Bess, J., N. Fujimoto, J. Sterbentz, L. Snoj, and A. Zukeran, *Evaluation of Zero-Power, Elevated Temperature Measurements at Japan's High Temperature Engineering Test Reactor*, INL/EXT-10-19627, March 2011.
- [9] Pope, M. A., J. Ortensi, and A. M. Ougouag, "Investigation of Supercells for Preparation of Homogenized Cross Sections for Prismatic Deep Burn VHTR Calculations," *5th International Conference on High Temperature Reactor Technology, HTR 2010*, October 2010.
- [10] Descotes, V., M. A. Pope, J. Ortensi, and A. Hebert, "Studies of 2-D Reflector Effects in Cross Section Preparation for Deep Burn VHTRs," *Nuclear Engineering and Design*, Vol. 242, pp. 148–156, January 2012.
- [11] Marleau, G., A. Hebert, and R. Roy, *A User Guide for Dragon Version5*, Technical Report IGE-335, Ecole Polytechnique de Montreal, 2016.
- [12] K. S. Smith, "Assembly Homogenization Techniques for Light Water Reactor Analysis," *Progress in Nuclear Energy*, Vol. 17, pp. 303–335, 1986.
- [13] A. Kavenoky, "The SPH Homogenization Method," *Proceedings of a Specialists' Meeting on Homogenization Methods in Reactor Physics, Lugano, Switzerland, November 13–15, 1978*, IAEA-TECDOC-231, p. 181, International Atomic Energy Agency, 1980.
- [14] A. Hébert, "A Consistent Technique for the Pin-by-Pin Homogenization of a Pressurized Water Reactor Assembly," *Nuclear Science and Engineering*, Vol. 113, pp. 227–238, 1993.
- [15] Hébert, A. and G. Mathonniere, "Development of a Third-Generation Superhomogenization Method for the Homogenization of a Pressurized Water Reactor Assembly," *Nuclear Science and Engineering*, Vol. 115, pp. 129–141, 1993.
- [16] Ortensi, J., "Prismatic Core Coupled Transient Benchmark," *Transactions of the American Nuclear Society*, Vol. 104, p. 854, 2011.
- [17] Rabiti, C., Y. Wang, G. Palmiotti, H. Hiruta, J. Cogliati, and A. Alfonsi, "PHISICS: A New Reactor Physics Analysis Toolkit," *Transactions of the American Nuclear Society*, Vol. 104, p. 831, 2011.